Developmentally Delayed Epigenetic Reprogramming Underlying the Pathogenesis of Preeclampsia

Wei He[1,2$], Yuan Wei[3$], Xiaoli Gong[3$], Luyuan Chang[4$], Wan Jin[4$], Ke Liu[5$], Xinghuan Wang[6,7,8,9$], Yu Xiao[6,7,8,9], Wenjing Zhang[4], Qiong Chen[4], Kai Wu[4], Lili Liang[4], Jia Liu[4], Yawen Chen[4], Huanhuan Guo[4], Xiaojuan Li[4], Wenhao Chen[4], Jiexia Yang[2], Yiming Qi[2], Yi Zhang[4,10,11#], and Aihua Yin[2#]

1. The First Affiliated Hospital of Jinan University, Guangzhou, China;

2. Medical Genetic Center, Guangdong Woman and Children Hospital, Guangzhou, China;

3. Department of Obstetrics and Gynecology, Peking University Third Hospital, Beijing, China;

4. Euler Technology, Beijing, China;

5. Department of Medical Oncology, Changzheng Hospital, Naval Medical University, Shanghai, China;

6. Department of Urology, Zhongnan Hospital of Wuhan University, Wuhan,China;

7. Department of Biological Repositories, Zhongnan Hospital of Wuhan University, Wuhan, China;

8. Human Genetic Resources Preservation Center of Hubei Province, Wuhan, China;

9. Laboratory of Precision Medicine, Zhongnan Hospital of Wuhan University, Wuhan, China;

10. Peking-Tsinghua Center of Life Sciences, Beijing, China;

11. School of Life Sciences, Peking University, Beijing, China;

$ These authors contribute equally to the paper.

Correspondence authors. Email: yinaiwa@vip.126.com, zy@eulertechnology.com.

Word Count: Summary 199; Main Text 2505.

Summary

Preeclampsia, a life-threatening pregnancy complication characterized by hypertension and multiorgan damage, affects 2-5% of pregnancies and causes 76,000 deaths per year. Most preeclampsia associated syndromes immediately dispel after removal of placenta, indicating a casual role of placenta in the pathogenesis. Failed transformation of spiral artery due to insufficient invasion and excessive apoptosis of trophoblast in preeclampsia placenta suggested developmental defects. However, the underlying molecular mechanisms that affected placenta development in preeclampsia remained elusive. Here we show that, in preeclampsia placenta, the bimodal epigenetic landscape formed during extraembryonic tissue differentiation was disrupted. ZGA-active NFYA/NFYB transcription factor binding were decreased, and NFY-bound LTR12 retrotransposons associated with VCT-specific genes were hypermethylated. Meanwhile, hundreds of EVT-specific gene promoters, which otherwise undergone *de novo* methylation in ExE, were hypomethylated and hyper-activated. DNA methylation defects were enriched on PcG-controlled loci in trophectoderm, resulted in a developmentally delayed placenta in preeclampsia. The preeclampsia-placenta-like methylation landscape could be detected in serum cell-free DNA from preeclampsia pregnant females starting from 13w GA. Preeclampsia could be accurately predicted from cfDNA methylation in independent retrospective and prospective cohorts. Our data suggests that the preeclampsia placenta represents a stalled state of epigenetic reprogramming *en route* of development from trophectoderm to normal placenta.

Dramatic epigenetic transformation occurs during human embryogenesis[1–8]. After zygote formation, the overall epigenome was turned into an open, transcriptionally permissive environment[2] by genome-wide removal of DNA methylation and H3K27me3 repressive mark[1,3,7] until zygote genome activation (ZGA) when repressive epigenetic modifications were re-established on linage-specification genes by maternal and ZGA-active[6,9,10] transcription factor priming, polycomb group protein (PcG) binding[11,12, 13,14,15,16], and *de novo* DNA methylation on CpG-island promoters[17]. In extraembryonic tissue (ExE), *de novo* methylation primes trophoblast cell lineage for implantation. Defective development of placenta results in failed transformation of spiral arteries caused by insufficient invasion of extravillous trophoblast (EVT) to the maternal uterus decidua[18] and excessive apoptosis of villous cytotrophoblast (VCT)[19]. The resulted insufficient supply of blood and hypoxia leads to reflective secretion of vasodilative factors such as s-FLT1 from placenta[20], causing an avalanche of pathological events leading to hypertension and multiorgan failure in preeclampsia[21]. To understand how placenta development is disrupted in preeclampsia, we assessed single cell and bulk genome-wide DNA methylation, histone modification and chromatin accessibility from different stages of human embryonic development to placenta, including single gamete (sperm and oocyte), zygote, 2-cell stage, 4-cell stage, 8-cell stage, morula, inner cell mass and trophectoderm from blastocyst stage, primed embryonic stem cells (ESC), trophoblast cells and preeclampsia- or non-preeclampsia placenta using a collection of data[1–4,6,22–24] (Extended Data Table S1).

Chromatin accessibility and TFBS changes in preeclampsia placenta

Global chromatin accessibility landscape differentiates placenta of preeclampsia pregnancy to normal ones (Extended Data Figure 1). Statistically significant difference on chromatin accessibility was identified on 3512 genomic loci, in which 1813 peaks are gain in preeclampsia (preeclampsia-gain) and 1698 are loss in preeclampsia (preeclampsia-loss) (Extended Data Table S2). These preeclampsia-specific, differentially regulated loci are particularly enriched for active TSS, CpG-islands, polycomb regulated regions and enhancers[11,12] (Figure 1a), suggesting a possibility that these regions were under control of DNA methylation [25]. Functionally, these loci are associated with known pathways for placenta development and function such as NOTCH3, VEGFA, MET, FOXO, ECM proteoglycan regulation, and coagulation (Figure 1b). Loci with significant chromatin accessibility changes are positioned in strategic locations for genes such as *PAPPA2*, *FLT1*, *LIFR*, *KDR*, *VEGFA* and *PGF* (Extended Data Figure 2), many of which were implicated in preeclampsia etiology as biomarkers[20,26,27], conferred genetic susceptibility[28–30], or with direct functional link[31–35]. These results are concordant to previous studies with RNA expression[36,37] and protein expression[20,26].

Transcription factor footprinting analysis[38,39] shows that binding of NFYA and NFYB, two key transcription factors regulating zygotic genomic activation (ZGA)[6,9], were down-regulated in preeclampsia placenta (Figure 1c-e), suggesting that ZGA might affect chromatin accessibility changes in preeclampsia. Consistently, peaks on preeclampsia-gain loci were usually found in pre-ZGA to early-ZGA embryonic stages, and preeclampsia-loss loci were more frequently found starting from early- to post-ZGA (Figure 1f), denoting a delayed evolution of epigenome landscape.

Methylation changes in preeclampsia placenta correlated to polycomb binding site in trophectoderm

TSS and CpG islands, two main genomic elements regulated by DNA methylation, were enriched for ATAC-seq changes in preeclampsia. We went on to analyze genome-wide methylation from fetal and maternal surface of placentas. To this end, we identified 4,418 differentially methylated regions (DMR) spatially segregated on genome, in which 2710 are hypomethylated (preeclampsia-hypo) and 1271 are hypermethylated (preeclampsia-hyper) in preeclampsia placenta compared to normal (Extended Data Table S3 and Extended Data Figure 3). Preeclampsia-hypo DMR were spatially segregated, but preeclampsia-hyper DMR were scattered across the genome (Extended Data Figure 4a-c). DNA reads on DMR were classified into high-methylation (methylated) and low-methylation (demethylated) haplotype based on the overall methylation frequency they carried with a Gaussian mixture model. On most DMR, the difference between preeclampsia and normal placentas are dominated by one single class of methylation haplotype. These DMR are highly specific such that they could distinguish preeclampsia placenta from not only normal ones but also the ones with other pregnancy complications such as gestational hypertension, gestational diabetes, and twin-twin transfusion syndrome (Figure 2a).

ExE-specific *de novo (ExE-de-novo)* methylated regions were dominated by preeclampsia-hypo DMR. Specifically, the mammalian conserved ExE-de-novo methylated region (Extended Data Figure 5) which showed hypermethylation in both human cancer sample (Figure 2b) and preeclampsia placenta (Figure 2c). Furthermore, this argument holds true for human-specific ExE-de-novo methylated region (Figure 2d and 2e). On the contrary, preeclampsia-hyper DMR does

not distinguish cancer to normal samples (Figure 2f and 2g). Enrichment analysis showed that the preeclampsia-hyper DMR were enriched with retrotransposons with long terminal repeat (LTR) and preeclampsia-hypo DMR are associated with gene promoters (Extended Data Figure 6). Among retrotransposons, the primate-specific LTR12 family[23] were dominated by preeclampsia-hyper DMR (Figure 2h and 2i). Up to 30% of LTR12C and LTR12D retrotransposons contain preeclampsia-hyper DMR (Figure 2h), and most LTR12C-contained DMR are hypermethylated in preeclampsia placenta (Figure 2i and Extended Data Figure 7a). LTR12 was known to be hypomethylated in primate sperm[23] and is considered as a primate-specific innovation of imprinting. We found that human sperm hypomethylated LTR12 were invariably hypermethylated in preeclampsia (Extended Data Figure 7b).

To understand the underlying molecular mechanism of differential methylation in preeclampsia, we analyzed histone modification profiles on these preeclampsia-associated DMR using existing Cut-And-Run histone modification data from different embryonic stages[2,4]. H3K4me3 modification on preeclampsia-associated DMR showed bimodal changes at early-ZGA stage (Figure 2j), with more H3K4me3-positive preeclampsia-hypermethylated regions (including LTR12C) and H3K4me3-negative preeclampsia-hypomethylated regions. The landscape of H3K4me3 on preeclampsia-hypermethylated regions were established with active transcription, as transcriptional blocking (TBE) halts the evolution of H3K4me3 modification pattern from 4-cell stage to 8-cell stage [2] (Figure 2j). On the other hand, for H3K27me3, bimodal changes were found in trophectoderm, with most preeclampsia-hypermethylated regions were H3K27me3-negative, and preeclampsia-hypomethylated regions were H3K27me3-positive (Figure 2k). These results suggest that DNA methylation defects in preeclampsia occurs on lineage-specifying genes under active regulation by PcG during placenta development.

Preeclampsia-hypermethylated regions are associated with VCT/SCT-specific genes and ZGA-active LTR12 retrotransposon

Fetal extraembryonic tissue builds placenta by providing villous cytotrophoblast (VCT)[40] which forms the major structure of fetal face of placenta, and differentiates along divergent trajectories toward either syncytiotrophoblast (SCT)[41], or extravillous trophoblast (EVT)[41]. Successful transformation of spiral artery requires coordinated, efficient generation of trophoblasts of both lineages. Using trophoblast single cell RNA sequencing data[22], we built a pseudotime evolution trajectory of VCT towards EVT or SCT using DMR-associated genes (Figure 3a, inset) . Most preeclampsia-hyper DMR associated genes were highly expressed in VCT (Figure 3a, large) and to a lesser extent SCT and decidua EVT, but not in the placental EVT, suggesting preeclampsia-hyper DMR might regulate VCT-specific or SCT-related genes. Concordant to this finding, on the fetal side of placenta, we found that the methylation haplotype frequency and overall methylation level of preeclampsia-hyper DMR, but not preeclampsia-hypo DMR, could differentiate placentas of preeclampsia pregnancy from normal ones (Figure 3b), suggesting the cell type enriched in fetal side of placenta as the major contributor of the methylated haplotypes in preeclampsia-hyper DMR. Together, these results suggest preeclampsia-hyper DMR might implicate in VCT (and SCT) function.

We used Monocle[42] to infer preeclampsia-hyper DMR associated gene expression level along the trophoblast differentiation trajectories (Figure 3c). By projecting cells on this pseudotime evolution trajectory, we found a subset of genes with associated LTR12C containing preeclampsia-hyper DMR were selectively expressed in VCT. During embryonic development, transcription from these LTR12C were selectively activated at ZGA (8-cell stage) (Figure 1f, and Figure 3d), whilst the NFYA/NFYB transcription factors[6,9] were most active and LTR12C were marked with

permissive histone marker H3K4me3 (Figure 2j). Methylation differences between preeclampsia-non-preeclampsia on these LTR12C elements were very similar (Figure 3d), with preeclampsia-specific hypermethylation at the 5' end of retrotransposon. These sites are devoid of methylation until early-ZGA stages (Extended Data Figure 7c and 7k). Hence, hypermethylation of these sites suggested a possibility that these retrotransposons were dysregulated before or during ZGA.

Many of the LTR12C hypermethylated in preeclampsia were with permissive histone mark in early ZGA and repressive histone mark re-established in trophectoderm (Figure 2j, 2k). For example, in *PAPPA2* (Extended Data Figure 7) *CDKN3* (Figure 3f) and *YY1* (Figure 3g), the adjacent hypermethylated LTR12C was active during 8-cell stage and repressed in trophectoderm. Analyzing chromatin interaction between the cognate promoters of these genes and the hypermethylated LTR12C showed an anti-correlation between LTR12C hypermethylation and transcriptional activation: *PAPPA2*, which is upregulated in preeclampsia[26] (Extended Data Figure 7), is associated with a hypermethylated LTR12C in its adjacent transcriptional activation domain (TAD) as suggested by chromatin interaction frequency; in contrast, *CDKN3*[43] and *YY1*[44] which are downregulated in preeclampsia (Figure 3E, F) are associated with a hypermethylated LTR12C in their own TAD. These results suggest that preeclampsia-specific hypermethylation of LTR12C might result in down-regulation of transcriptional activity in the TAD, and up-regulates transcriptional activity in the adjacent TADs.

Post-ZGA-active, embryonically protected CpG island promoters associated with EVT-specific genes were hypomethylated

We used a similar strategy to locate the cell type(s) most affected by preeclampsia-hypo DMR. Preeclampsia-hypo DMR associated genes were exclusively expressed in EVT (Figure 4a),

without significant expression in either SCT or VCT. Meanwhile, methylation levels of preeclampsia-hypo DMR could differentiate the maternal side, but not fetal side, of preeclampsia placenta from normal ones (Figure 4b). Pseudotime model was built with Monocle to infer preeclampsia-hypo DMR associated gene expression level along the trophoblast differentiation trajectories (Figure 4c). In contrast to the preeclampsia-hyper DMR associated genes, many preeclampsia-hypo DMR associated genes such as *FLT1, FGFR3, E2F8 and DOCK5* were selectively expressed in EVT only (Figure 4c). The preeclampsia-hypo DMR associated with these genes are generally located in the promoter or enhancer elements, and are closely associated with regions with preeclampsia-gain of chromatin accessibility (Extended Data Figure 8).

Preeclampsia-specific gains of chromosomal accessibility of these genes were exclusively found in placenta, but not earlier developmental stages (Extended Data Figure 9, and Figure 2), implicating that these chromatin openings formed no earlier than TE-to-ExE transition. Since ExE-specific *de novo* methylation of promoters is non-cell-autonomous [17] , preeclampsia-specific hypomethylation on these genomic loci implies a failure of *de novo* methylation during TE-to-ExE transition, which in turn suggests an early defect at the time of implantation[17] .

In all EVT-expressed genes, the preeclampsia-associated gene *FLT1* is of particular interest because it was biochemically[20] and genetically[28] linked to preeclampsia, and was found to be directly causing a preeclampsia-like phenotype in transgenic animal model downstream of endometrium VEGF[33]. We found preeclampsia-specific enhancers for *FLT1* by gain of chromatin accessibility and loss of DNA methylation on H3K27ac-marked loci (Figure 4d). These enhancer encompassed the known fetal genome susceptibility locus rs4769613 and rs12050029 for preeclampsia[28] and were conformationally linked to alternative *FLT1* promoters (Figure 4d). Moreover, these enhancers were marked with re-established H3K27me3 in trophectoderm (Figure

4e), suggesting that *FLT1* were directly targeted by PcG[45] during TE-to-ExE transformation and loss of such regulation may result in s-FLT1 overexpression (Figure 4f).

Stalled epigenetic reprogramming of placenta in preeclampsia

Together, we conclude that specific epigenomic changes in preeclampsia placenta occurs on linage-specification related chromatin loci, leads to dysregulation of ZGA-active LTR12 family retrotransposon, and post-ZGA defect of TE-to-ExE transformation. These observations leads us to hypothesize that whether failed epigenetic reprogramming underlies the defective development of the preeclampsia placenta[46]. We tested this hypothesis by projecting placenta bulk methylation or ATAC sequencing results onto the evolution landscape built with single cell sequencing data. Mapping DNA methylation data positioned preeclampsia placenta along the innate developmental trajectory from trophectoderm cells towards trophoblast, whilst normal placenta clustered with *ex vivo* induced trophoblast (differentiated cells derived from trophectoderm) (Figure 5a). Similarly, using chromatin accessibility on DMR regions (Extended Data Figure 10), we found that unlike the normal placenta which clustered together with endogenous trophoblast, preeclampsia placenta was positioned along the trajectory from trophectoderm towards trophoblast (Figure 5b). Altogether, these results suggest that preeclampsia placenta is developmentally delayed not only anatomically, but also epigenetically.

In vivo evidence for the early stalled development of placenta from cell-free DNA

So far, we draw analysis based on sequencing data from term placenta. Due to continuous post-implantation development, these data might not accurately reflect the epigenomic landscape at earlier gestational stages. Serum cell-free DNA (cfDNA) originated from apoptotic cells in human body[47]. In early stages of pregnancy, cfDNA from pregnant female contains DNA of fetal origin[48],

which retains their original covalent chemical modification[49,50]. We hypothesized that sequencing cfDNA methylation profile from pregnant female, at very early gestational age, might be used to deduce the placental developmental status. If so, sequencing cfDNA methylation profile at early gestational weeks might predict pregnancy outcome.

We sequenced the DNA methylation profiles on preeclampsia-associated DMR from cell-free DNA from 15-20w GA (gestational age) blood draws of 20 pregnant females and 10 nongravida females. Analyzing the methylation haplotypes carried by sequencing reads showed that normal-placenta associated (Figure 6a) methylation haplotype on these DMR could be readily detected in cfDNA of female of normal, but not preeclampsia, pregnancy (Figure 6a). Similarly, preeclampsia-placenta associated methylation haplotypes could be only detected in samples from pregnancy females who latter developed preeclampsia (Figure 6b and 6c). Because these methylation haplotypes were never observed in nongravida female, they represent placenta-specific biomarkers which could be used to non-invasively track placental development.

To validate that early gestational week cfDNA methylation profile could be used to predict preeclampsia in later stage, we conducted a double-blinded, retrospective validation experiment. We firstly built a general linear model to convert the sequenced cfDNA profile as a quantitative measure of placenta development to predict pregnancy outcome, which showed a 100% accuracy to predict preeclampsia in this small cohort. Blood draws collected at 13-20w GA, originally for NIPT, from 159 pregnant females, in which 37 were of preeclampsia, were used to validate the model. Methylation profiles of these cfDNA were captured and sequenced. Pregnancy outcome prediction based on methylation haplotype profiling achieved a 97% sensitivity and 89% specificity in this cohort (Figure 6d). Post-hoc analysis showed that, starting from 13w GA, the

cfDNA methylation profile from females who latter developed preeclampsia was significantly delayed compared to normal ones (Figure 6e).

Finally, we prospectively collected blood draws from two females at their early pregnancy to perform methylation profiling. Consecutive blood draws from 13-17w GA showed stable methylation profile measurement (Figure 6f), suggesting that the evolution of methylation profile of placental genome might be largely finished at 13w GA. Furthermore, we found the measurement accurately predicted their pregnancy outcome (Figure 6g).

Discussion and Conclusion

Placenta, as the maternal-fetal interface, is essential for fetal development. Although it was known for decades that anatomical defective placental development underlies the pathogenesis of serious pregnancy complications such as fetal growth restriction and preeclampsia, their underlying molecular mechanism are largely unknown. Here we showed that preeclampsia is a disease associated with developmentally delayed placenta accompanied with failed epigenetic reprogramming characterized by specific DNA methylation and chromatin accessibility defects which together affected development of trophoblasts, and stalled the evolution of preeclampsia epigenome along its innate developmental trajectory. Application of low dose aspirin before 16w GA may protect 50-70% of early-onset preeclampsia incidence in high-risk groups. Our results does not only provided insights into preeclampsia etiology, but also provided a mean for accurate identification of these high risk female at early GA weeks.

Author Contributions

Y.Z, and A.H.Y conceived and designed the study. W.H., Y.W., X.L.G., J.X.Y, and Y.M.Q. collected clinical placenta and serum samples. Y.Z., K.L., X.H.W., and Y.X. arranged and collected clinical tumor and normal tissue samples. W.H. collected the clinical data for pregnant female, and set blinding for the validation cohort. W.J. collected the prospective prediction samples and their associated clinical data, performed table statistics on clinical data. Y.Z., Q.C., W.H.C., K.W. and H.H.G. developed the *Tequila 7N* single-stranded methylation sequencing assay. W.J. and K.W. collected, dissected, and processed placenta samples for ATAC-seq. K.W., L.L.L., L.Y.C., Q.C., J.L., Y.W.C. and W.H.C. collected, dissected, and processed placenta samples for methylation capture sequencing. K.W., L.L.L., L.Y.C., Q.C., J.L., Y.W.C., H.H.G., Y.X. and W.H.C. collected, dissected, and processed tumor and normal tissue samples for methylation capture sequencing. K.W., L.L.L., L.Y.C., Q.C., J.L., Y.W.C. and W.H.C. processed plasma samples for methylation capture sequencing. Y.Z., L.Y.C., W.J.Z. and X.J.L. designed and implemented the methylation sequencing bioinformatic analysis pipeline. W.J.Z. performed the conservation analysis of methylation data between mouse and human. L.Y.C. and Y.Z. designed and implemented the methylation capture panel oligo design pipeline. L.Y.C. designed the methylation capture panel. L.L.L. produced and quality-controlled the methylation capture panel. Y.Z. designed and implemented the ATAC-seq and histone modification bioinformatic analysis pipelines. Y.Z. and W.J.Z. performed the single cell bioinformatic analysis. Y.Z. performed the TF footprint analysis. Y.Z., L.Y.C., and W.J.Z. built the statistical model for cell-free DNA methylation sequencing and performed analysis for the clinical validation test. Y.Z. and W.J wrote the paper with input from all authors.

Acknowledgements

The authors would like to thank Dr. Yi Rao for comments on the manuscript. This study is funded by National Key R&D Program of China (2016YFC1000700, 2016YFC1000703 to A.H.Y. and 2016YFC1000400 to Y.W.), Department of Science and Technology of Guangdong Province (2016A030313787 to A.H.Y), and research fund from Euler Technology, Beijing, China.

Conflict of interest declaration

Provisional patents were filed for the single-stranded NGS library preparation method *Tequila 7N* (WO 2020/073748) and the method for using cell-free DNA methylation pattern to predict placenta development status and pregnancy outcome (202010084924.X).

Reference

1. Zhu, P. *et al*. Single-cell DNA methylome sequencing of human preimplantation embryos. *Nat. Genet*. **50**, 12–19 (2018).

2. Xia, W. *et al*. Resetting histone modifications during human parental-to-zygotic transition. *Science (80-.)*. **365**, 353–360 (2019).

3. Zhou, F. *et al*. Reconstituting the transcriptome and DNA methylome landscapes of human implantation. *Nature* **572**, 660–664 (2019).

4. Wu, J. *et al*. Chromatin analysis in human early development reveals epigenetic transition during ZGA. *Nature* **557**, 256–260 (2018).

5. Gao, L. *et al*. Chromatin Accessibility Landscape in Human Early Embryos and Its Association with Evolution. *Cell* **173**, 248-259.e15 (2018).

6. Liu, L. *et al*. An integrated chromatin accessibility and transcriptome landscape of human pre-implantation embryos. *Nat. Commun*. **10**, 1–11 (2019).

7. Ziller, M. J. *et al*. Charting a dynamic DNA methylation landscape of the human genome. *Nature* **500**, 477–481 (2013).

8. Guo, H. *et al*. The DNA methylation landscape of human early embryos. *Nature* **511**, 606–610 (2014).

9. Lu, F. *et al*. Establishing chromatin regulatory landscape during mouse preimplantation development. *Cell* **165**, 1375–1388 (2016).

10. De Iaco, A. *et al*. DUX-family transcription factors regulate zygotic genome activation in placental mammals. *Nat. Genet*. **49**, 941–945 (2017).

11. Ernst, J. & Kellis, M. ChromHMM: Automating chromatin-state discovery and characterization. *Nat. Methods* **9**, 215–216 (2012).

12. Ernst, J. & Kellis, M. Chromatin-state discovery and genome annotation with ChromHMM. *Nat. Protoc*. **12**, 2478–2492 (2017).

13. Chen, Z., Yin, Q., Inoue, A., Zhang, C. & Zhang, Y. Allelic H3K27me3 to allelic DNA methylation switch maintains noncanonical imprinting in extraembryonic cells. *Sci. Adv*. **5**, (2019).

14. van Heeringen, S. & Akkers, R. Principles of nucleation of H3K27 methylation during embryonic development. *Genome Res*. **24**, 401–410 (2014).

15. Zheng, H. *et al*. Resetting Epigenetic Memory by Reprogramming of Histone Modifications in Mammals. *Mol. Cell* **63**, 1066–1079 (2016).

16. Saxena, M. *et al*. Transcription factor-dependent 'anti-repressive' mammalian enhancers exclude H3K27me3 from extended genomic domains. *Genes Dev*. **31**, 2391–2404 (2017).

17. Smith, Z. D. *et al*. Epigenetic restriction of extraembryonic lineages mirrors the somatic

transition to cancer. *Nature* **549**, 543–547 (2017).

18. Lyall, F., Robson, S. C. & Bulmer, J. N. Spiral artery remodeling and trophoblast invasion in preeclampsia and fetal growth restriction relationship to clinical outcome. *Hypertension* **62**, 1046–1054 (2013).

19. Tomas, S. Z., Prusac, I. K., Roje, D. & Tadin, I. Trophoblast apoptosis in placentas from pregnancies complicated by preeclampsia. *Gynecol. Obstet. Invest.* **71**, 250–255 (2011).

20. Maynard, S. E. *et al*. Excess Placental Soluble fms-like Hypertension , and Proteinuria in preeclampsia. *J. Clin. Invest.* **111**, 649–58 (2003).

21. Wisner, K. Gestational Hypertension and Preeclampsia. *MCN Am. J. Matern. Nurs.* **44**, 170 (2019).

22. Vento-Tormo, R. *et al*. Single-cell reconstruction of the early maternal–fetal interface in humans. *Nature* **563**, 347–353 (2018).

23. Molaro, A. *et al*. Sperm methylation profiles reveal features of epigenetic inheritance and evolution in primates. *Cell* **146**, 1029–1041 (2011).

24. Gamage, T. K. J. B. *et al*. Human trophoblasts are primarily distinguished from somatic cells by differences in the pattern rather than the degree of global CpG methylation. *Biol. Open* **7**, (2018).

25. Bianco-Miotto, T. *et al*. Recent progress towards understanding the role of DNA methylation in human placental development. *Reproduction* **152**, R23–R30 (2016).

26. Macintire, K. *et al*. PAPPA2 is increased in severe early onset pre-eclampsia and upregulated with hypoxia. *Reprod. Fertil. Dev.* **26**, 351–357 (2014).

27. Zeisler, H. *et al*. Predictive value of the sFlt-1:PlGF ratio in women with suspected preeclampsia. *N. Engl. J. Med.* **374**, 13–22 (2016).

28. McGinnis, R. *et al*. Variants in the fetal genome near FLT1 are associated with risk of preeclampsia. *Nat. Genet.* **49**, 1255–1260 (2017).

29. Low, P. & Variants, F. Protective low frequency variants for preeclampsia in the FLT1 gene in the Finnish population. **70**, 365–371 (2018).

30. Amin-Beidokhti, M. *et al*. An intron variant in the FLT1 gene increases the risk of preeclampsia in Iranian women. *Clin. Exp. Hypertens.* **41**, 697–701 (2019).

31. Stewart, C. L., Kaspart, P. & Brunet, L. J. Blastocyst Implantation Depends on Maternal Expression of Leukaemia Inhibitory Factor. *Nature* **2664**, 265–268 (1992).

32. Adelman, D. M., Gertsenstein, M., Nagy, A., Simon, M. C. & Maltepe, E. Placental cell fates are regulated in vivo by HIF-mediated hypoxia responses. *Genes Dev.* **14**, 3191–3203 (2000).

33. Fan, X. *et al*. Endometrial VEGF induces placental sFLT1 and leads to pregnancy complications. *J. Clin. Invest.* **124**, 4941–4952 (2014).

34. Shore, V. H. *et al*. Vascular endothelial growth factor, placenta growth factor and their receptors in isolated human trophoblast. *Placenta* **18**, 657–665 (1997).

35. Wang, H. Y., Zhang, Z. & Yu, S. Expression of PAPPA2 in human fetomaternal interface and involvement in trophoblast invasion and migration. *Genet. Mol. Res.* **15**, 1–16 (2016).

36. Ashar-Patel, A. *et al*. FLT1 and transcriptome-wide polyadenylation site (PAS) analysis in preeclampsia. *Sci. Rep.* **7**, 1–14 (2017).

37. Thomas, C. P., Andrews, J. I. & Liu, K. Z. Intronic polyadenylation signal sequences and alternate splicing generate human soluble Fltl variants and regulate the abundance of soluble Flt1 in the placenta. *FASEB J.* **21**, 3885–3895 (2007).

38. Corces, M. R. *et al*. The chromatin accessibility landscape of primary human cancers. *Science (80-.).* **362**, (2018).

39. Li, Z. & Schulz, M. Identification of transcription factor binding sites using Gaussian mixture models. *Genome Biol.* **31**, 70–80 (2014).

40. Turco, M. Y. *et al*. Trophoblast organoids as a model for maternal–fetal interactions during human placentation. *Nature* **564**, 263–281 (2018).

41. Lyall, F., Bulmer, J. N., Kelly, H., Duffie, E. & Robson, S. C. Human trophoblast invasion and spiral artery transformation. The role of nitric oxide. *Am. J. Pathol.* **154**, 1105–1114 (1999).

42. Qiu, X. *et al*. Reversed graph embedding resolves complex single-cell trajectories. *Nat. Methods* **14**, 979–982 (2017).

43. Garrido-Gomez, T. *et al*. Severe pre-eclampsia is associated with alterations in cytotrophoblasts of the smooth chorion. *Dev.* **144**, 767–777 (2017).

44. Tian, F. J. *et al*. The YY1/MMP2 axis promotes trophoblast invasion at the maternal-fetal interface. *J. Pathol.* **239**, 36–47 (2016).

45. Inoue, A., Jiang, L., Lu, F., Suzuki, T. & Zhang, Y. Maternal H3K27me3 controls DNA methylation-independent imprinting. *Nature* **547**, 419–424 (2017).

46. Nizyaeva, N. V. *et al*. Ultrastructural and Immunohistochemical Features of Telocytes in Placental Villi in Preeclampsia. *Sci. Rep.* **8**, 1–15 (2018).

47. Lui, Y. Y. N. *et al*. Predominant hematopoietic origin of cell-free dna in plasma and serum after sex-mismatched bone marrow transplantation. *Clin. Chem.* **48**, 421–427 (2002).

48. Dennis Lo, Y. M. *et al*. Presence of fetal DNA in maternal plasma and serum. *Lancet* **350**, 485–487 (1997).

49. Tsui, D. W. Y., Chiu, R. W. K. & Dennis Lo, Y. M. Epigenetic approaches for the detection of fetal DNA in maternal plasma. *Chimerism* **1**, 30–35 (2010).

50. Tong, Y. K. *et al*. Noninvasive prenatal detection of trisomy 21 by an epigenetic-genetic chromosome-dosage approach. *Clin. Chem.* **56**, 90–98 (2010).

a

Element Type	All	Overall ATAC Difference	Gain in Preeclampsia	Loss in Preeclampsia	Percent Gain in Preeclampsia	Percent Loss in Preeclampsia
Active TSS	18422	192	108	84	0.005862556	0.004559765
CpG island	28691	170	91	79	0.003171726	0.002753477
Weak Repressed PolyComb	36018	189	113	76	0.00313732	0.002110056
Weak transcription	110506	735	340	395	0.003076756	0.003574467
Transcripts at gene 5 and 3	679	5	2	3	0.002945508	0.004418262
Bivalent Enhancer	10425	39	22	17	0.002110312	0.001630695
Flanking Bivalent TSS Enhancer	7118	24	15	9	0.002107334	0.0012644
Enhancers	119230	477	248	229	0.002080013	0.001920658
Strong transcription	33323	145	65	80	0.001950605	0.002400744
Flanking Active TSS	17065	69	32	37	0.001875183	0.00216818
Genic enhancers	8162	32	14	18	0.001715266	0.002205342
Bivalent Poised TSS	3614	11	6	5	0.00166021	0.001383509
Repressed PolyComb	15998	32	18	14	0.001125141	0.000875109
ZNF genes and repeats	14193	19	14	5	0.000986402	0.000352286
Heterochromatin	42046	70	39	31	0.000927556	0.000737288

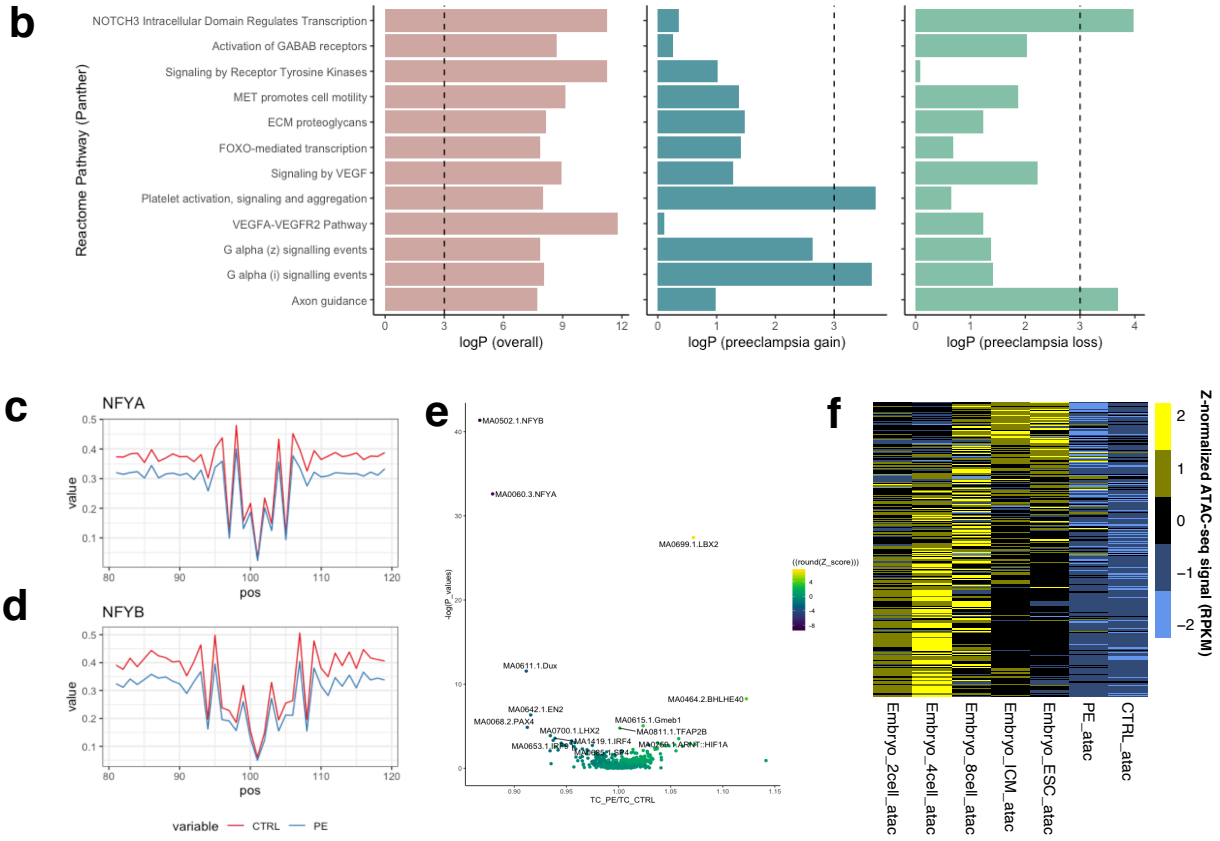

Figure 1: Chromatin accessibility of preeclampsia placenta showed bimodal defects associated with specific developmental stage

a). Enrichment of significantly different ATAC-seq peaks on different classes of[11,12] chromHMM genomic regions. b). Enrichment of significantly ATAC-seq peaks on Reactome Pathways from PantherDB. Significantly enriched pathway with FDR < 0.01 were shown on the figure. X axis: log P value (unadjusted); dashed line: P=0.001. Left/pink: gene pathways associated with peaks with significant differences; Middle/dark green: genes associated with preeclampsia-gained peaks; Right/olive: genes associated with preeclampsia-lost peaks. c). Transcription factor footprint of

NFYA is significantly decreased in preeclampsia. X axis: position (100=TF binding site) around the TF binding site for NFYA; Y axis: normalized read depth; Red: non-preeclampsia (CTRL) placenta; Blue: preeclampsia (PE) placenta. d). Transcription factor footprint of NFYB is significantly decreased in preeclampsia; X axis: position (100=TF binding site) around the TF binding site for NFYB; Y axis: normalized read depth; Red: non-preeclampsia (CTRL) placenta; Blue: preeclampsia (PE) placenta. e). Scatter plot denoting the ratio of TF footprint strength for preeclampsia over normal placenta (X-axis) and P-value (Y-axis) for TF binding differences on placenta. X axis: Difference of read depth ratio of preeclampsia-vs.-non-preeclampsia placenta; Y axis: log P value. Color hue: Z from -8 to 4. f). Z-normalized ATAC signal (RPKM) intensity across embryonic stages on IDR peaks showed differences between preeclampsia and non-preeclampsia placenta.

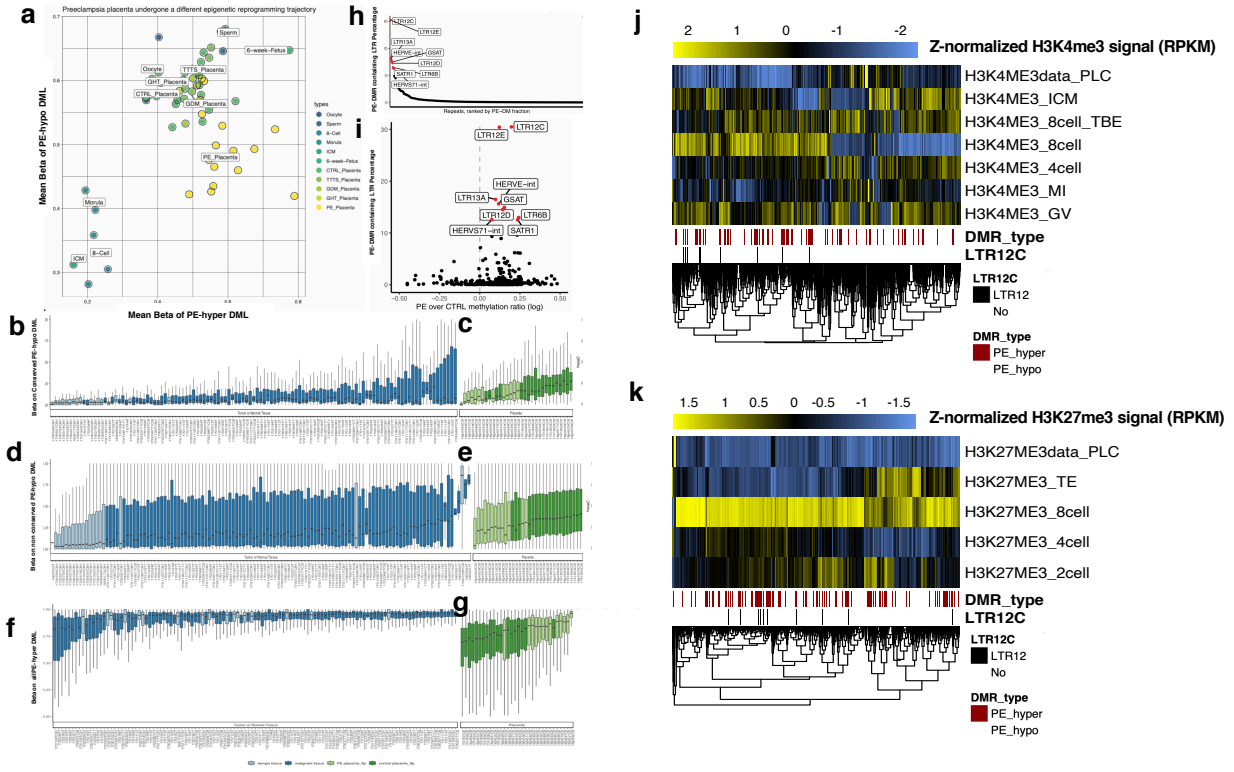

Figure 2: Bimodal genome-wide methylation defects associated with preeclampsia

a). Mean methylation level (beta) of PE-hyper (X) and PE-hypo (Y) loci distinguishes preeclampsia samples from other non-preeclampsia placenta and embryo samples. Color: samples of different embryonic stages or types of placenta. GHT: gestational hypertension; GDM: gestational diabetes; TTTS: twin-twin transfusion syndrome; PE: preeclampsia; b-c). Box-and-whisker plot of methylation level (beta) of mammalian conserved PE-hypo DML on individual samples; light blue: normal samples; dark blue: tumor samples. light green: preeclampsia fetal surface placenta samples; dark green: normal fetal surface placenta samples. d-e) Box-and-whisker plot of methylation level (beta) of non-conserved, human-specific PE-hypo DML on individual samples; light blue: normal samples; dark blue: tumor samples. light green: preeclampsia fetal surface placenta samples; dark green: normal fetal surface placenta samples. f-g) Box-and-whisker plot of methylation level (beta) of all PE-hyper DML on individual samples; light blue: normal samples; dark blue: tumor samples. light green: preeclampsia fetal surface placenta samples; dark green: normal fetal surface placenta samples. h). LTR12 retrotransposon family were the most affected repeat element in preeclampsia placenta. Y-axis: Percentage of repeat element containing preeclampsia-specific DMR; X-axis: rank of percentage from high to low; Red dots with names are repeats with significant enrichment (Fisher's exact test P<0.05) of DMR j). LTR12 family retrotransposon are hypermethylated in preeclampsia placenta. X-axis: log-ratio of mean methylation level of preeclampsia placenta over normal placenta for individual class of repeat element; Y-axis: Fractions of repeats containing preeclampsia-specific DMR. Red dots with names are repeats with significant enrichment (Fisher's exact test P<0.05) of DMR. j). Z-normalized H3K4me3 Cut-and-Run signal (RPKM) within +- 100bp of preeclampsia-specific DMR across different embryonic stages and placenta samples showed transcriptional-dependent enrichment of H3K4me3 mark on preeclampsia-hyper and LTR12C DMR in 8-cell-stage. PLC: Placenta; ICM:

inner cell mass; TBE: transcriptional block; MI: meiosis I oocyte; GV: geminal vesicle. k). Z-normalized H3K27me3 Cut-and-Run signal (RPKM) +- 10000bp of preeclampsia-specific DMR across different embryonic stages and placenta samples showed exclusion of H3K27me3 mark on preeclampsia-hyper and LTR12C DMR in trophectoderm. PLC: Placenta; TE: trophectoderm. Black lines: LTR12C-contained DMR; Red lines: preeclampsia-hyper DMR;

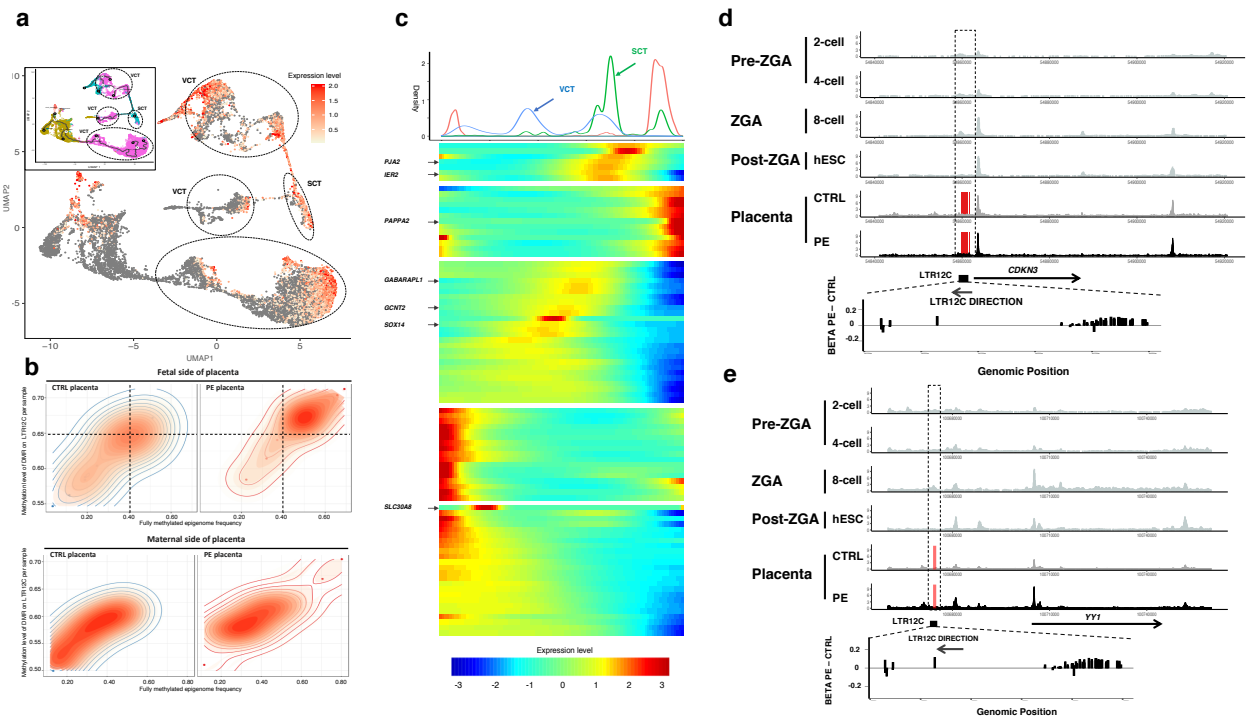

Figure 3: Genomic region hypermethylated in preeclampsia placenta are associated with VCT- and SCT-specific genes and ZGA-active retrotransposon

a). UMAP projection and pseudotime trajectory (black) of single-cell RNA sequencing results of trophoblasts. Heat color denotes sum of preeclampsia-hyper DMR associated gene expression level in each cell. Inset: color-coded classes of trophoblasts. pink: VCT; blue: SCT; yellow: EVT; red: decidua EVT. b). Preeclampsia-hyper DMR methylation level (Y) and fully-methylated DNA read frequency (X) are different between preeclampsia and normal placenta on the fetal, but not maternal surface. Individual placenta samples were denoted as dots, and 2-d distribution were outlined. c). Gene expression level modelled on pseudotime trajectory for preeclampsia-hyper DMR associated genes. Top: distribution of cells at different timepoints (x-axis) of pseudotime. Blue: VCT; Red: EVT; Green: SCT. d). ATAC-seq of 2-cell, 4-cell, 8-cell, primed-ESC, preeclampsia (PE) and normal (CTRL) placenta on CDKN3 loci. Red background denotes DMR location. Dashed box denotes a preeclampsia-hypermethylated LTR12C in CDKN3 which is transcriptionally activated at early-ZGA (8-cell). Lower panel: methylation level difference of CpG in the LTR12C element, between preeclampsia and normal placenta. Direction of LTR12C were denoted as arrow. e). ATAC-seq of 2-cell, 4-cell, 8-cell, primed-ESC, preeclampsia (PE) and normal (CTRL) placenta on YY1 loci. Red background denotes DMR location. Dashed box denotes a preeclampsia-hypermethylated LTR12C in YY1 which is transcriptionally activated at early-ZGA (8-cell). Lower panel: methylation level difference of CpG in the LTR12C element, between preeclampsia and normal placenta. Direction of LTR12C were denoted as arrow.

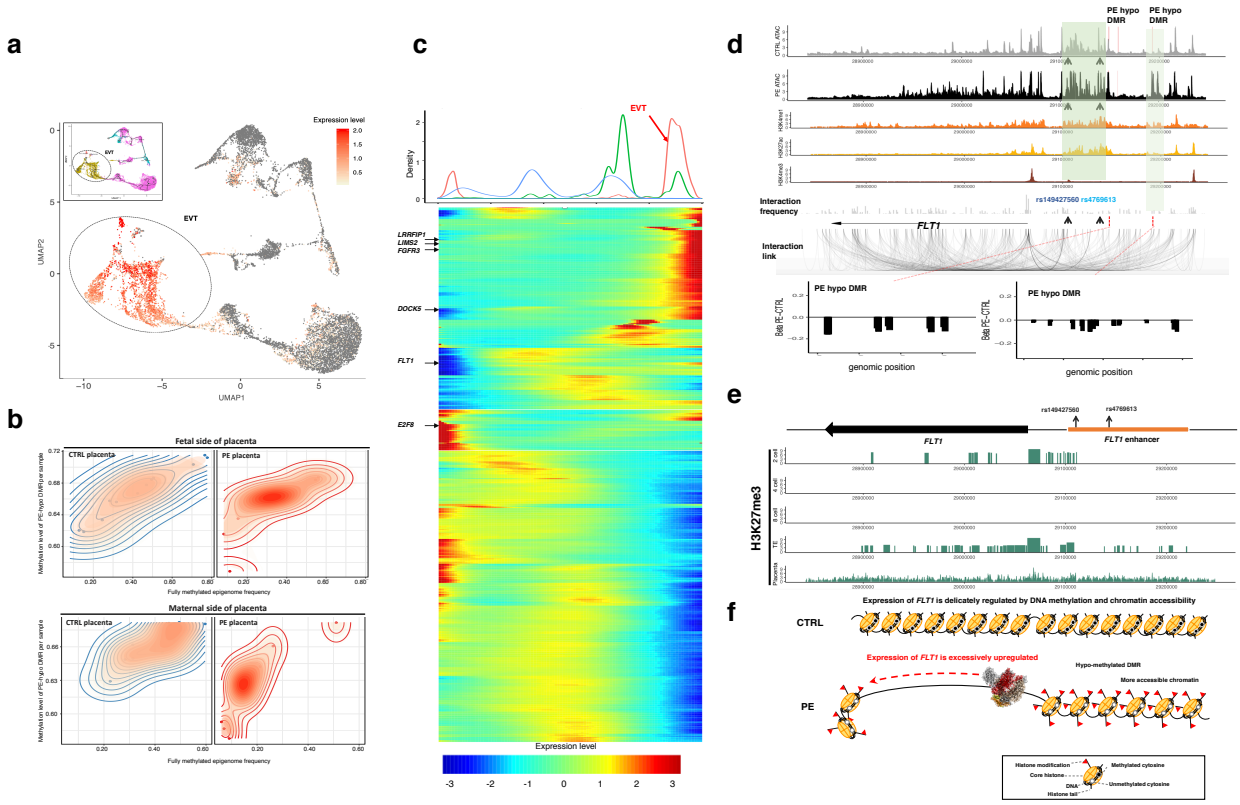

Figure 4: Post-ZGA-active, embryonically protected CpG island promoters associated with EVT-specific genes were hypomethylated in preeclampsia placenta

a). UMAP projection and pseudotime trajectory (black) of single-cell RNA sequencing results of trophoblasts. Heat color denotes sum of preeclampsia-hypo DMR associated gene expression level in each cell. Inset: color-coded classes of trophoblasts. pink: VCT; blue: SCT; yellow: EVT; red: decidua EVT. b). Preeclampsia-hypo DMR methylation level (Y) and fully-methylated DNA read frequency (X) are different between preeclampsia and normal placenta on the maternal, but not fetal surface. Individual placenta samples were denoted as dots, and 2-d distribution were outlined. c). Gene expression level modelled on pseudotime trajectory for preeclampsia-hypo DMR associated genes. Top: distribution of cells at different timepoints (x-axis) of pseudotime. Blue: VCT; Red: EVT; Green: SCT. d). ATAC-seq of preeclampsia (PE) and normal (CTRL) placenta, and associated H3K4me3, H3K27ac, H3K4me1 modification ChIP-seq signal on *FLT1* loci. Red dashed line denotes preeclampsia-hypo DMR location. Green shadow box denotes a preeclampsia-gained enhancer for FLT1. Positions for variants associated with increased risk for preeclampsia were denoted. Middle panel: Chromatin interaction intensity (gray histogram) and individual chromatin interaction links (bottom curves) on the region, showing that the preeclampsia-gained enhancer interacts with poised and regular promoter of FLT1. Lower panel: methylation level difference of CpG in the preeclampsia-hypo DMR, between preeclampsia and normal placenta. e). H3K27me3 modification (Cut-and-Run for embryo, and ChIP-seq for placenta) level on the same region, showing that the preeclampsia-gained enhancer was under control of PcG and marked by H3K27me3 at trophectoderm stage. f). Schematic drawing for epigenetic mechanism controlling FLT1 overexpression in preeclampsia.

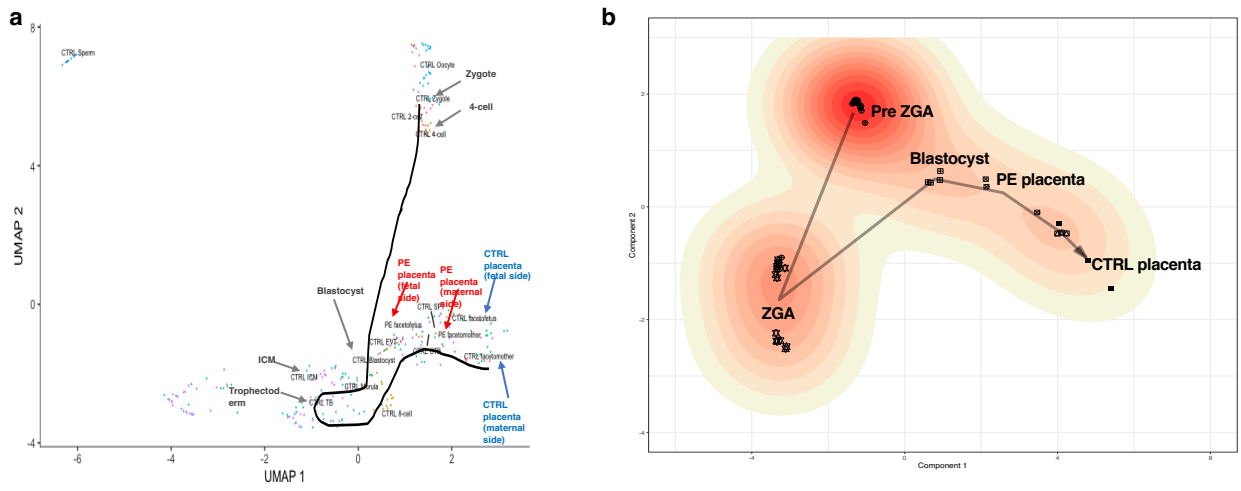

Figure 5: Stalled placenta epigenome development in preeclampsia

a). UMAP and pseudotime trajectory for single cell and bulk tissue methylome sequencing from different embryonic stages to placenta, showing that preeclampsia placentas are stalled en route of the trajectory from blastocyst to trophoblast. b). UMAP and pseudotime trajectory for single cell and bulk tissue ATAC sequencing from different embryonic stages to placenta, showing that preeclampsia placentas are stalled *en route* of the trajectory from blastocyst to trophoblast.

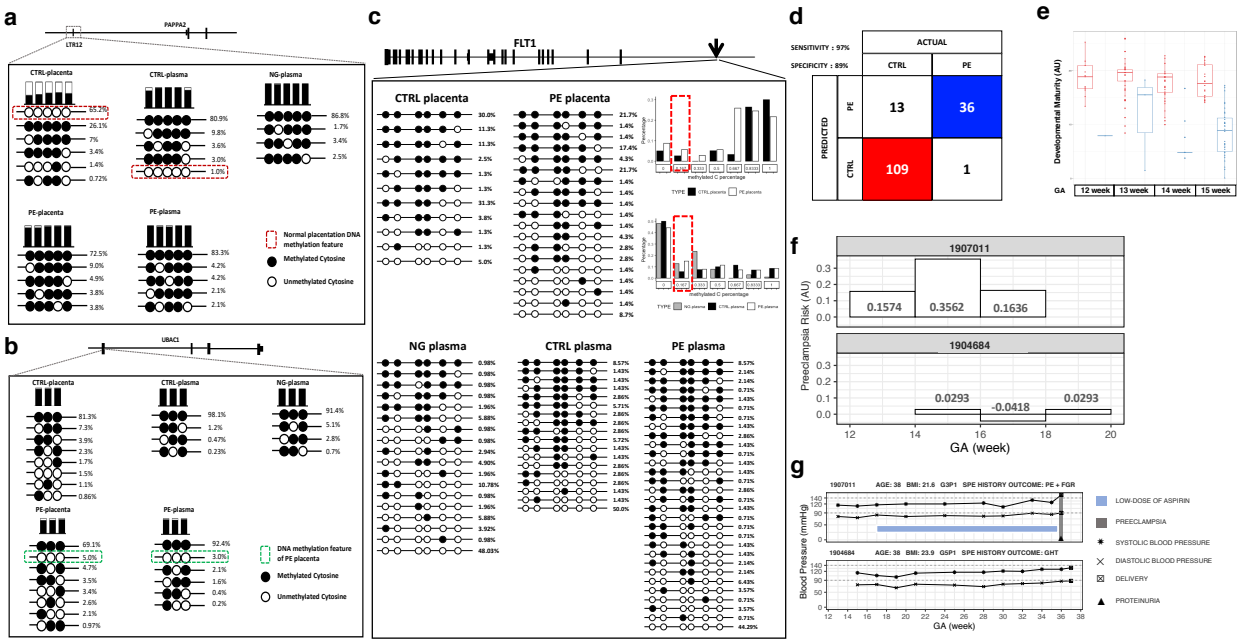

Figure 6: In vivo evidence for the early stalled development of placenta in cell-free DNA

a). Normal pregnancy associated methylation haplotype on a preeclampsia-hyper DMR on LTR12C element 5' of PAPPA2 could be detected in cell-free DNA. Mean methylation level (beta: top columns. black: methylated, white: unmethylated), individual CpG-loci methylation combinations on DNA sequencing reads (methylation haplotype, bottom panels) and associated frequency of each methylation haplotype (figures on the right) were shown for control placenta, preeclampsia placenta, control pregnant female, preeclampsia pregnant female, and nongravida female. Red dashed box denotes the normal pregnancy associated methylation haplotype which could only be found in placenta or cell-free DNA from control pregnant female. b). Preeclampsia pregnancy associated methylation haplotype on a preeclampsia-hypo DMR 5' of UBAC1 could be detected in cell-free DNA. Green dashed box denotes the preeclampsia pregnancy associated methylation haplotype which could only be found in placenta or cell-free DNA from preeclampsia pregnant female. c). Preeclampsia-specific methylation haplotypes with lower methylation level (statistics in inset bar graphs) on FLT1 preeclampsia-specific enhancer detected in cell-free DNA. d). Sensitivity and specificity in blinded validation for predicting preeclampsia with cell-free DNA methylation haplotype in a retrospective cohort. e). Post-hoc analysis showing predicted placenta developmental maturity is lower in preeclampsia individuals at early GA weeks. (Y-axis) Predicted placenta developmental maturity with cell-free DNA methylation haplotype from female who latter developed preeclampsia (blue) or normal (red). (X-axis) GA weeks. f). Prospective prediction of preeclampsia risk (Y-axis) from consecutive blood draws of two volunteers. g). Clinical outcome of the two volunteers, showing that the methylation haplotype deduced preeclampsia risk could predict final clinical outcome.